Radiometric Comparison of 1.6-μm CO_2 Absorption Band of *Greenhouse Gases Observing Satellite* (*GOSAT*) TANSO-FTS with *Suomi-NPP* VIIRS SWIR Band

SIRISH UPRETY

Cooperative Institute for Research in the Atmosphere, Colorado State University, Fort Collins, Colorado

CHANGYONG CAO

Center for Satellite Applications and Research, NOAA/NESDIS, College Park, Maryland

(Manuscript received 4 August 2015, in final form 9 May 2016)

ABSTRACT

An atmospheric CO_2 increase has become a progressively important global concern in recent past decades. Since the 1950s, the Keeling curve has documented the atmospheric CO_2 increase as well as seasonal variations, which also intrigued scientists to develop new methods for global CO_2 measurements from satellites. One of the dedicated satellite missions is the CO_2 measurement in the 1.6-μm shortwave infrared spectra by the *Greenhouse Gases Observing Satellite* (*GOSAT*) Thermal and Near Infrared Sensor for Carbon Observations–Fourier Transform Spectrometer (TANSO-FTS) instrument. While this spectral region has unique advantages in detecting lower-trophosphere CO_2, there are many challenges because it relies on accurate measurements of reflected solar radiance from Earth's surface. Therefore, the calibration of the TANSO-FTS CO_2 has a direct impact on the CO_2 retrievals and its long-term trends. Coincidently, the *Suomi-NPP* Visible Infrared Imaging Radiometer Suite (VIIRS) 1.6-μm band spectrally overlaps with the TANSO-FTS CO_2 band, and both satellites are in orbit with periodical simultaneous nadir overpass measurements. This study performs an intercomparison of VIIRS and the TANSO-FTS CO_2 band in an effort to evaluate and improve the radiometric consistency. Understanding the differences provides feedback on how well the *GOSAT* TANSO-FTS is performing over time, which is critical to ensure a well-calibrated, stable, and bias-free CO_2 product.

1. Introduction

Global climate change has been a major concern for scientists, industrialists, politicians, as well as private citizens because it is believed that at least part of the global change is due to anthropogenic activities such as the mass consumption of fossil fuels in industrial activities as well as daily mass transportation. While debates continue about the rate of global change and trends in the different layers of the atmosphere, the CO_2 increase in the atmosphere has been consistently increasing since the 1950s as suggested by the Keeling curve (http://www.esrl.noaa.gov/gmd/ccgg/trends/full.html) from ~310 ppm in 1950s to ~400 ppm at the end of 2014, which is one of the most convincing evidence of anthropogenic contributions to climate change. It is also interesting to note that the achievements of the Keeling endeavor, which earned presidential awards, highly rely on SI unit traceability of the instrument calibration and the long-term consistency in the measurements. Over the last recent decades, the instruments used for the CO_2 measurements have changed many times for deriving the Keeling curve. Maintaining the consistency and SI traceability has been critical for the credibility and success of the Keeling curve. It should also be noted that before the SI unit traceability of the Keeling curve was established in the 1950s, there were many CO_2 studies with numerous measurements. Unfortunately, all the results were not consistent. In fact, some studies suggested that the CO_2 in the 1930s was already more than 400 ppm at the time (Slocum 1955),

Corresponding author address: Sirish Uprety, Cooperative Institute for Research in the Atmosphere, Colorado State University, 1375 Campus Delivery, Fort Collins, CO 80523.
E-mail: sirish.uprety@noaa.gov; changyong.cao@noaa.gov

DOI: 10.1175/JTECH-D-15-0157.1

which later was found not credible. From this perspective, accuracy in instrument calibration is crucial to climate studies.

The success of the Keeling observations of CO_2 intrigued many scientists in the science community. However, a major limitation of the Keeling methodology is that it is based on point measurements at a specific location (the Mauna Loa, Hawaii, site). Global studies of CO_2 with satellite observations had been the dream of many scientists but were largely limited by instrumentation. It is true that atmospheric CO_2 has been of great interest for atmospheric sounders since the 1970s, as in the CO_2 channels of the High Resolution Infrared Radiation Sounder (HIRS) series from 1979 to the present, as well as the Stratospheric Sounding Unit (SSU), which uses CO_2 pressure cells on orbit for calibration. However, those instruments were mostly limited to atmospheric temperature measurements using CO_2 absorption features. There was also the short-lived Infrared Interferometer Spectrometer (IRIS) in the 1970s, and the Interferometric Monitor for Greenhouse Gases (IMG) in the late 1990s, which had the potential for CO_2 retrievals. It was not until the launch of hyperspectral infrared sounders, such as AIRS (on *Aqua* since 4 May 2002), the Infrared Atmospheric Sounding Interferometer (IASI; since 2006 on MetOp), the *Greenhouse Gases Observing Satellite* (*GOSAT*; since 2009), and the Cross-track Infrared Sounder (CrIS; since 2011), did routine global retrievals of CO_2 concentration from satellite measurements become a reality.

Following the infrared hyperspectral sounders, instrumentation has been developed in the near infrared in the last decade that focuses specifically on CO_2 retrievals in the 1.6- and 2.0-μm spectral region as demonstrated by *GOSAT* and the Orbiting Carbon Observatory (OCO) instruments. While this approach offers unique advantages for CO_2 retrievals with finer spatial and spectral resolution, vertical CO_2 layers down to near the surface, and less contamination from other gases, it also relies on several parameters such as molecular absorption line parameters and aerosol-related parameters. The accuracy of XCO_2 and XCH4 retrieval from the *GOSAT* Thermal and Near Infrared Sensor for Carbon Observations—Fourier Transform Spectrometer (TANSO-FTS) depends on the absolute calibration accuracy of the instrument. For the thermal infrared (TIR) band, a blackbody is used as a calibration source because it is highly accurate and stable. However, for solar reflective bands, maintaining accurate radiometric calibration is always a challenge mainly due to the degradation in optics and the onboard calibration system such as a solar diffuser. This is one of the reasons why vicarious calibration is performed on TANSO-FTS solar bands almost every year: to evaluate and improve the instrument calibration stability and absolute accuracy (Kuze et al. 2012, 2014, 2016; Kina et al. 2010; Shiomi et al. 2007). Poor calibration of TANSO-FTS solar bands can lead to higher uncertainties in the estimation of retrieval inputs that in turn leads to larger uncertainty in CO_2 retrievals. The importance of accurate radiometric calibration of TANSO-FTS solar bands in CO_2 retrieval has been described in a number of earlier studies (Kuze et al. 2009a, 2012, 2014; Yoshida et al. 2011, 2012). The effective optical pathlength for CO_2 retrieval depends on a number of parameters, such as surface albedo, scattering albedo, surface pressure, aerosol optical thickness, and cloud-top height. These parameters can be estimated accurately from measurements only if the instrument is well calibrated in absolute scale. To meet the observation requirement for CO_2 retrieval, surface albedo and aerosol retrieval requires an accuracy of absolute radiometric calibration better than 5% (Kuze et al. 2009a). Several studies have been performed in the past to improve the radiometric calibration accuracy of TANSO-FTS (Yoshida et al. 2012; Kuze et al. 2012, 2014).

This study examines the consistency between the Visible Infrared Imaging Radiometer Suite (VIIRS) 1.6-μm band and the corresponding *GOSAT* TANSO-FTS band with the goal to assess their relative accuracy, consistency, and long-term trend. The study directly addresses the recommendations of the Committee on Earth Observation Satellites (CEOS) as documented in CEOS (2014) for the actions supporting carbon data product intercomparisons and cross calibration. In the following, section 2 provides a methodology description (the instruments used in the study and the techniques used in comparing instruments) and section 3 presents the results. It concludes with section 4.

2. Methodology

It is recognized in the science community that generally, the calibration uncertainties for the reflective solar bands, including the shortwave infrared band such as at 1.6-μm, are much greater than that for the thermal infrared bands, partly due to the uncertainties in the onboard calibration sources and the variability of the phenomena observed, such as the sun–satellite geometry correction. There are significant differences in the calibration between thermal infrared sounders versus shortwave infrared instruments. Thermal infrared sounders measure emitted radiances from the atmosphere and surfaces, while shortwave infrared instruments measure solar radiances reflected by the surface and atmosphere. This fundamental difference led to several calibration-related issues that in turn affected the retrieved CO_2

trends. First, the current state of the art in the onboard blackbody calibration uncertainty of thermal infrared bands is typically on the order of 0.1 K (at 300 K or approximately 0.15% at 12 μm), while in the shortwave infrared, the calibration uncertainty is on the order of 1%–3% with onboard calibration or higher with vicarious calibration. Second, the reflected solar radiance varies greatly with time and location compared to emitted radiances from Earth and the atmosphere, which are within a relatively narrower range. For example, VIIRS thermal emissive band M16 at 12 μm measures radiance ranging from nearly 4 to nearly 10 $W m^{-2} sr^{-1} \mu m^{-1}$ over targets varying from polar snow to hot desert compared to a shortwave infrared (SWIR) band such as M10 at 1.6 μm that measures radiance varying from less than 0.2 $W m^{-2} sr^{-1} \mu m^{-1}$ over dark ocean to greater than 35 $W m^{-2} sr^{-1} \mu m^{-1}$ over desert. Third, the shortwave infrared retrieval of CO_2 relies on the knowledge of surface reflectance and stability in the trends, which in turn relies on the calibration of these bands; while in the thermal infrared, this is less of a concern because the temperature monitor for blackbody is not degraded. Even though the calibration for TIR is more stable, the retrieval is more complex mainly because the algorithm needs an accurate vertical temperature profile. On the other hand, even though the SWIR band can be used to more accurately retrieve CO_2 due to a simpler algorithm, the long-term stability is poor mainly due to more complexity and more challenging radiometric calibration. More rigorous calibration is needed for the reflective solar bands to meet the stringent accuracy requirements in the CO_2 retrieval from the 1.6-μm band.

The comparison of the VIIRS and TANSO-FTS 1.6-μm bands will provide insight into the relative accuracy and stability of the two instruments, which may have implications on the CO_2 retrievals in terms of accuracy and trends because the surface reflectance is used in the CO_2 retrieval from TANSO-FTS. The comparison will also benefit VIIRS because TANSO-FTS is hyperspectral, which can potentially help reduce spectral uncertainties in the comparison.

a. *VIIRS and TANSO-FTS instruments*

VIIRS is one of the key Earth-observing remote sensing instruments on board the *Suomi National Polar-Orbiting Partnership* (*Suomi-NPP*) satellite, which was successfully launched on 28 October 2011 from Vandenberg Air Force Base (VAFB) in California. It is a cross-track scanning radiometer that measures emitted and reflected radiation from Earth and the atmosphere, covering wavelengths from 0.4 to 12 μm. VIIRS has three types of bands: 5 imagery bands (I bands, 375-m resolution at nadir), 16 moderate-resolution bands (M bands, 750-m resolution at nadir), and the day/night band (750-m resolution across scan). Of particular interest to this study are the 1.6-μm bands, which are designed primarily to observe cloud and ice. Similar to all other reflective solar bands, the 1.6-μm band is calibrated using the onboard solar diffuser (SD). It is noted that although there is an onboard solar diffuser stability monitor (SDSM) that monitors the SD degradation, it only spans up to 0.9 μm and does not cover this band because it is assumed that the degradation of the SD in this spectral region is negligible. As a result, vicarious methods, including lunar calibration, are used to assess the SD degradation of this band. A detailed description of VIIRS can be found in Cao et al. (2013a). The VIIRS 1.6-μm bands (M10 and I3) are centered at 1.6 μm with sufficient spectral coverage for the CO_2 absorption feature that the TANSO-FTS covers.

GOSAT is a JAXA mission that was launched on 23 January 2009 and dedicated to greenhouse gas measurements. The payloads on *GOSAT* include the TANSO-FTS in both the shortwave infrared and thermal infrared. The TANSO-FTS has three bands in the visible/shortwave infrared centered at 0.76, 1.64, and 2.00 μm. A band for TANSO-FTS denotes the instrument line shape functions. Spectral bands of TANSO-FTS are defined with its dichroic beam splitters and bandpass filters. *GOSAT* also includes the TANSO–Cloud and Aerosol Imager (TANSO-CAI). The *GOSAT* has an orbital altitude of 666 km in a sun-synchronous orbit with the equator crossing at 1300 local crossing time (descending which is in the opposite direction of the typical NOAA afternoon satellites. A more detailed explanation of *GOSAT* instruments can be found in Kuze et al. (2009a,b) and Moreau et al. (2014).

In comparing the VIIRS and TANSO-FTS 1.6-μm band (Fig. 1), it should be recognized that different technologies are used in designing these instruments. For VIIRS, the instrument is a filter radiometer; while for TANSO-FTS, it is a Fourier transform spectrometer (FTS) with very fine spectral resolutions of 0.2 wavenumbers (about 0.05 nm at 1.6 μm). While TANSO-FTS has been commonly used for hyperspectral sounders such as IASI and CrIS in the infrared, the TANSO-FTS 1.6-μm band uses the same technology but applied to the shortwave infrared spectrum, which is to measure reflected sunlight instead of emitted radiance. In an FTS system, the incoming light is split into two beams by a beamsplitter into separate optical paths to create an optical path difference between the two. For TANSO-FTS, this optical path difference is created with swing arms mounted with retro reflectors on each arm. The two light beams are then recombined at the beamsplitter to cause interference. With the swing arm, the FTS

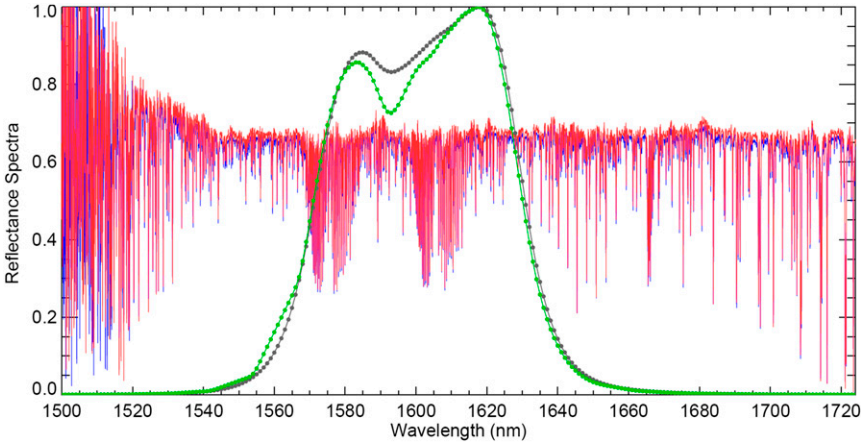

FIG. 1. *GOSAT* FTS reflectance spectra for *P* and *S* polarized reflectance over the Libyan Desert along with VIIRS M10 (black) and I3 (green) RSR.

measures the intensity of the interference by continuously changing the optical path difference, which produces an interferogram. The inverse Fourier transform of the interferogram produces the spectrum of the earth view. Unlike other typical interferometers, the TANSO-FTS also produces interferograms in the *P* and *S* polarizations. Figure 1 shows the TANSO-FTS reflectance spectra over the Libya-4 desert site for both *P* and *S* polarized light.

Note that the TANSO-FTS specified spectral range is from 1.5625 to 1.7241 μm. From Fig. 1 it is clear that the VIIRS M10 relative spectral response range extended farther to the left, outside of the nominal TANSO-FTS spectral range. On the other hand, the TANSO-FTS data are available for wavelengths wider than what is provided in the specification, although the noise increases greatly toward the shorter wavelength. At the same time, the VIIRS M10 spectral response is reduced greatly toward 1.5 μm. As a result, there is generally a good spectral overlap between the TANSO-FTS and VIIRS 1.6-μm bands.

b. *Methodology for comparing VIIRS and* GOSAT *TANSO-FTS observations at extended SNOs*

The simultaneous nadir overpass (SNO) method (Cao et al. 2004) has been widely used in the science community for the intersatellite calibration of radiometers on polar-orbiting satellites. It has also been used by scientists in constructing long-term time series for climate change detection studies, and the World Meteorological Organization (WMO) has adopted the SNO methodology as an essential element in its Global Space-Based Intercalibration System (GSICS) program. The methodology is conceptually straight forward. However, the concept of satellite intercomparison using near-simultaneous observations was implemented and published much earlier in the past, dating back to the 1980s (Kieffer et al. 1985; Metzler and Malila 1985). Kieffer et al. (1985) compared *Landsat-4* and *Landsat-5* using near-simultaneous measurements with a time difference of about 25 s. In the case of *GOSAT* and *Suomi-NPP*, since they fly at different altitudes in the polar orbits (830 km for *Suomi-NPP* and 666 km for *GOSAT*), there is an orbital period difference between the two satellites that creates opportunities for simultaneous nadir overpasses periodically. At the SNO, both VIIRS and TANSO- FTS are observing the same scene on the earth within a few seconds. Using the formula described in Cao et al. (2004), the occurrence of the SNOs between *GOSAT* and *Suomi-NPP* in the low latitudes ranges mostly once every 2–3 days. A number of publications exist from 1980s in which the two satellite instruments were compared to each other using near-simultaneous observations.

SNO events between *Suomi-NPP* and *GOSAT* are shown in Fig. 2a. Unlike typical SNOs where both satellites are flying in the same direction when the SNOs occur, in the case of *GOSAT* and *Suomi-NPP*, the two satellites are flying in opposite directions (Fig. 2b). This configuration leads to a much shorter time window at the SNOs than the typical scenario. It also limits the SNOs to primarily the tropics. It is worth noting that the SNOs between them occur in the low latitudes, which is especially useful for intercalibrating the two instruments with a large dynamic range over a variety of Earth scenes. This study uses SNOs over North African desert sites to perform an intercomparison primarily because the reflectance is relatively higher than other regions, such as ocean. The comparison is made over extended SNOs (SNO-x), that is, including the area away from the

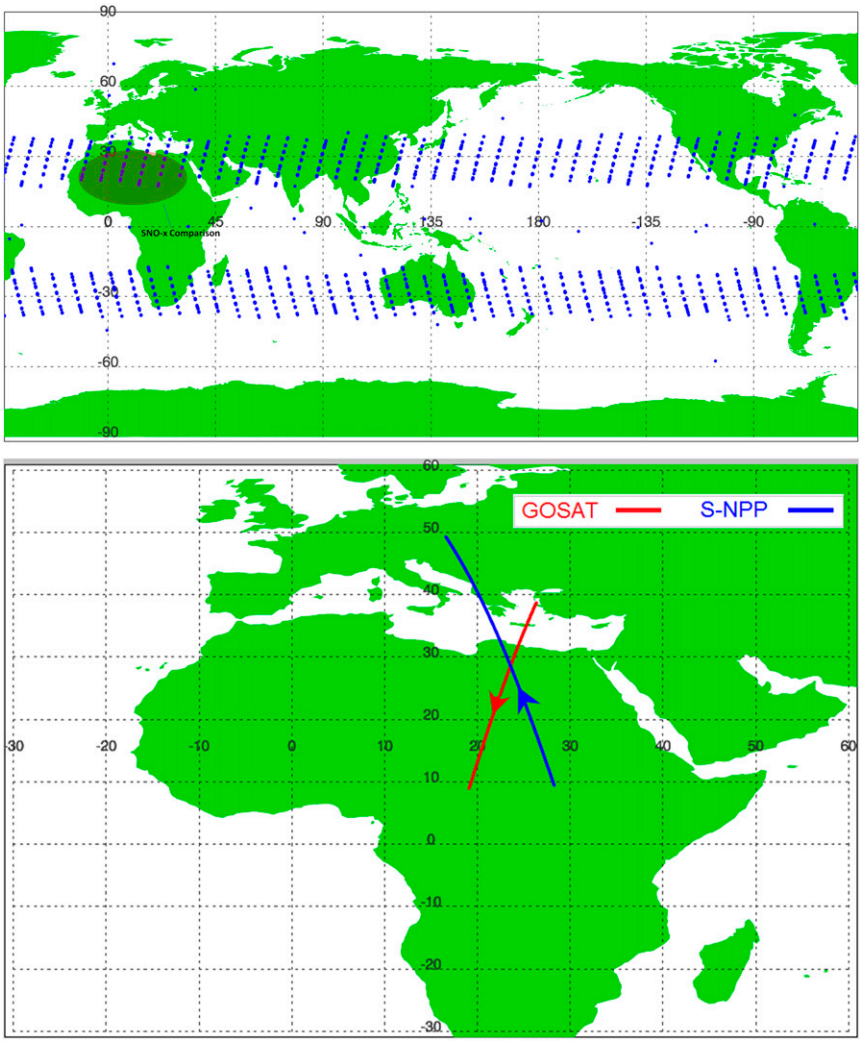

FIG. 2. (a) *GOSAT* and *Suomi-NPP* SNO events in a tropical region. (b) A sample SNO event with *GOSAT* and *Suomi-NPP* orbital intersection with orbital paths in opposite direction.

orbital intersection using the technique described in an earlier study by Uprety et al. (2013). This allows us to use more data points for each SNO. The details on data selection and screening procedure are described below.

In data processing, only data from 2013 to 2014 are used in this study because there were significant changes in the calibration in the early days of VIIRS on orbit. A radiometric comparison of VIIRS M10 and *GOSAT* TANSO-FTS is performed using extended SNO over African deserts. The processing steps for computing observed bias are described below.

1) SNO events and data collection

   The SNO events between *Suomi-NPP* and *GOSAT* were predicted and analyzed from 2013 until the end of 2014. For each SNO event, VIIRS data were collected from NOAA Comprehensive Large Array-Data Stewardship System (CLASS) archive (http://www.class.ncdc.noaa.gov) and TANSO-FTS L1B data were collected from the GOSAT data product website (https://data.GOSAT.nies.go.jp/gateway/gateway/MenuPage/open.do). A more detailed description of the level 1 data processing of TANSO-FTS can be found in Kuze et al. (2009b, 2012).

2) Extract collocated VIIRS regions of interest (ROIs) and TANSO-FTS observation

   VIIRS is an imaging radiometer that has measurements for each pixel (742 m) over the swath of about 3040 km. TANSO-FTS was designed with the capability to observe five points (or exposures) in a cross-track direction, but it has measurements for three exposures (points) typically with a spatial resolution of 10 km. For each SNO at the overlapping region of observation of VIIRS and TANSO-FTS, collocated

measurements are compared. For each TANSO-FTS point, a VIIRS circular ROI is extracted such that its size matches the TANSO-FTS point size and the center of each TANSO-FTS exposure matches the VIIRS ROI center. For each extended SNO event, there can be a number of VIIRS ROIs compared with matching TANSO-FTS points.

VIIRS L1B data products are available in both radiance and reflectance, whereas the TANSO–TANSO-FTS L1B product is available in radiance spectra only. The details on product format can be found in JAXA (2009). This study compares VIIRS and TANSO-FTS in the reflectance domain. Radiance spectra of TANSO-FTS (L_{ib}) are converted to the top-of-atmosphere (TOA) reflectance using the following equation:

$$\rho = \frac{\pi D_{se}^2}{\cos(\theta) E_{sun}}, \quad (1)$$

where θ denotes the solar zenith angle at the target of observation, L_{ib} denotes the TANSO-FTS radiance spectra for a given exposure or a point, D_{se} denotes the sun–earth distance at the time of observation in astronomical unit (AU), $\cos(\theta)$ denotes the cosine of the solar zenith angle, and E_{sun} denotes the in-band solar irradiance of TANSO-FTS. This study uses the Kurucz spectrum, which is interpolated at the TANSO-FTS center wavelength to be used for E_{sun} values.

We used the Kurucz spectrum to generate E_{sun} values for TANSO-FTS because *Suomi-NPP* VIIRS also uses the Kurucz spectrum (found in MODTRAN, version 4.3) in operational algorithms (Cao et al. 2013b). Kuze et al. (2014) have provided the degradation factors for all FTS bands. For each band, the degradation rate is not constant across all wavenumbers. Thus, wavenumber-based degradation correction is done by applying the scaling factors provided by Kuze et al. (2014). These degradation rates were computed using vicarious calibration and are available at particular wavelengths only. Thus, these values need to be interpolated to generate a lookup table (LUT) using a smooth function that covers the entire wavelength range of the given band. The spectral reflectance is convolved with the VIIRS M10 relative spectral response (RSR) to generate simulated VIIRS M10–equivalent reflectance of FTS with degradation correction. This band-averaged reflectance is then used to compare with the collocated VIIRS ROI to estimate the bias between the instruments.

For the ROIs to be valid, the following data filtering criteria are applied: 1) a sensor zenith $< 10°$, 2) a time difference < 15 min, 3) a cloud mask applied using the VIIRS intermediate cloud mask product, and 4) a spatial uniformity of VIIRS $< 5\%$.

3) Compute bias time series

For each SNO event, there can be many collocated ROIs over VIIRS images for TANSO-FTS exposures. A bias is calculated for the ROI as

$$\text{Radiometric bias} = (\text{VIIRS} - \text{FTS})100\%/\text{VIIRS}.$$

If there are N ROIs for an SNO event, then there will be N bias values for that event. All bias values (observed bias) for each SNO event are plotted as a function of time. This process is repeated for all SNO events. A linear fit on bias time series along with one-sigma residual standard deviation is used to analyze the bias time series and to evaluate the consistency between the VIIRS M10 and TANSO-FTS band 2 (1.6 μm).

c. *Method for comparing VIIRS and* GOSAT *TANSO-FTS observations at desert calibration sites*

While the intercomparion at the SNOs are very useful, the results are relative between the two instruments compared. Therefore, the observations from the two instruments are also compared at well-known calibration sites, such as desert sites. Since the sites are well characterized, the measurements at these sites provide a quasi-traceable calibration. In this comparison, the near-nadir observations of the VIIRS and *GOSAT* TANSO-FTS are collected. Only clear-sky data are used in the comparison. In addition, MODIS data are also used as a reference. Detailed procedures are described below.

This study uses the Libya-4 desert calibration site because this site has been well characterized and is widely used for calibration/validation of Earth-observing satellite instruments (Teillet et al. 2007; Helder et al. 2013, 2010; Markham and Helder 2012; Chander et al. 2010). In addition, this is one of the CEOS-endorsed calibration sites. TANSO-FTS has 3-day repeat cycle compared to VIIRS, which has a 16-day repeat cycle. Thus, TANSO-FTS observes the Libya-4 region at nadir for almost 5 times more than that of VIIRS. We have used only near-nadir view observations in the analysis. One of the limitations with TANSO-FTS is that, it does not necessarily observe the exact same point during every repeat cycle. The change in location of the TANSO-FTS observation is mainly due to the pointing instability of the instrument. Thus, the location of the TANSO-FTS observation can vary within

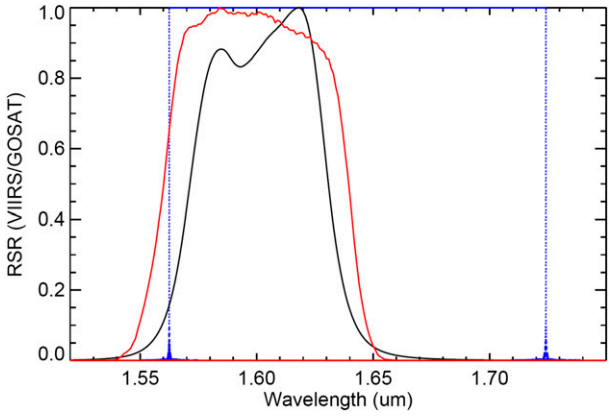

FIG. 3. FTS spectral coverage along with VIIRS M10 and I3 RSR.

the pointing instability unlike the VIIRS, which observes the exact same location of the earth during every repeat cycle. This study uses a fixed location for VIIRS at Libya-4 (28.55°N, 23.39°E). However, the observed location can vary for TANSO-FTS and is collected mainly from four different locations near Libya-4, and the impact of the intercomparison due to varying observing locations is analyzed in section 3a.

Figure 3 shows the VIIRS M10 RSR along with *GOSAT* TANSO-FTS spectral coverage and *GOSAT* CAI imager band 4 RSR. The figure shows that VIIRS M10 RSR is not completely covered by the TANSO-FTS spectral range, with a small section of VIIRS RSR that appears out of band (OOB) of the FTS band 2. This is not a major issue in the comparison because TANSO-FTS L1B data are available for a longer wavelength range (although maybe less accurate) than the specification.

Comparison over the desert site is performed using at-sensor TOA reflectance. The VIIRS data product is available in reflectance, whereas TANSO-FTS data are present in radiance and thus need to be converted to reflectance using the technique described in section 2b(3). Data processing basically involves the following steps:

1) A circular ROI with 10 km in diameter is extracted for VIIRS during each nadir overpass of the instrument over the site.
2) Filtering criteria are applied to each ROI of VIIRS:
   (i) Only the ROI with all clear-sky pixels are considered for analysis. The cloud mask product from VIIRS is used to determine the level of cloud contamination.
   (ii) Spatial uniformity–based criteria are used for cloud masking the VIIRS data. Each ROI is considered valid only if the spatial uniformity (ratio of one standard deviation to mean reflectance) of the ROI is better than 4%.
   (iii) A sensor zenith threshold of 10° for all pixels within an ROI is used to limit the analysis only within near nadir.

   After an ROI passes all the above-mentioned conditions, the mean and standard deviation are calculated and a temporal trend is generated for VIIRS. The following steps are used for TANSO-FTS:
3) A 3-day repeat cycle is used to collect near-nadir data. Data are downloaded from online (https://data.gosat.nies.go.jp/gateway/gateway/MenuPage/open.do).
4) Each exposure or point observed near the Libya-4 site is used in generating a reflectance time series. Equation (1) shows the equation for computing TOA reflectance for TANSO-FTS. Unlike SNO-x where both the VIIRS and TANSO-FTS observe the same Earth location at almost the same time, the two instruments observe the Libya-4 site on different days but at very close local time. The cloud mask product of VIIRS cannot be used to detect the cloud contamination for TANSO-FTS observed points due to the time difference in observation. To detect cloud over the TANSO-FTS points, *GOSAT* CAI data may be used. However, this study does not perform a cloud mask for TANSO-FTS.
5) Similar to VIIRS, a time series is generated using only near-nadir points by limiting the sensor zenith angle to less than 10°.

3. Results and discussion

Section 3a discusses the results of the VIIRS and TANSO-FTS intercomparison near the Libya-4 desert site. The relative bias between VIIRS and TANSO-FTS is analyzed. In addition, *Aqua* MODIS is used to assist in comparing the results. Similarly, section 3b provides the result of the SNO-x-based intercomparison over the North African desert. The relative accuracy and uncertainties in bias are analyzed.

a. Comparison over Libyan Desert

VIIRS and TANSO-FTS TOA reflectance time series are shown in Fig. 4a. Both VIIRS and TANSO-FTS show strong seasonal patterns in the TOA reflectance time series. This seasonal reflectance change is attributed to the desert bidirectional reflectance distribution function (BRDF). The figure clearly indicates that VIIRS and TANSO-FTS agree well with each other; however, it is interesting to note that there is a bias between the *P* and *S* polarization measurements. The TANSO-FTS time series also suggest larger scatter. The two possible reasons are 1) no cloud mask is used and 2) as explained in section 2c,the TANSO-FTS observations

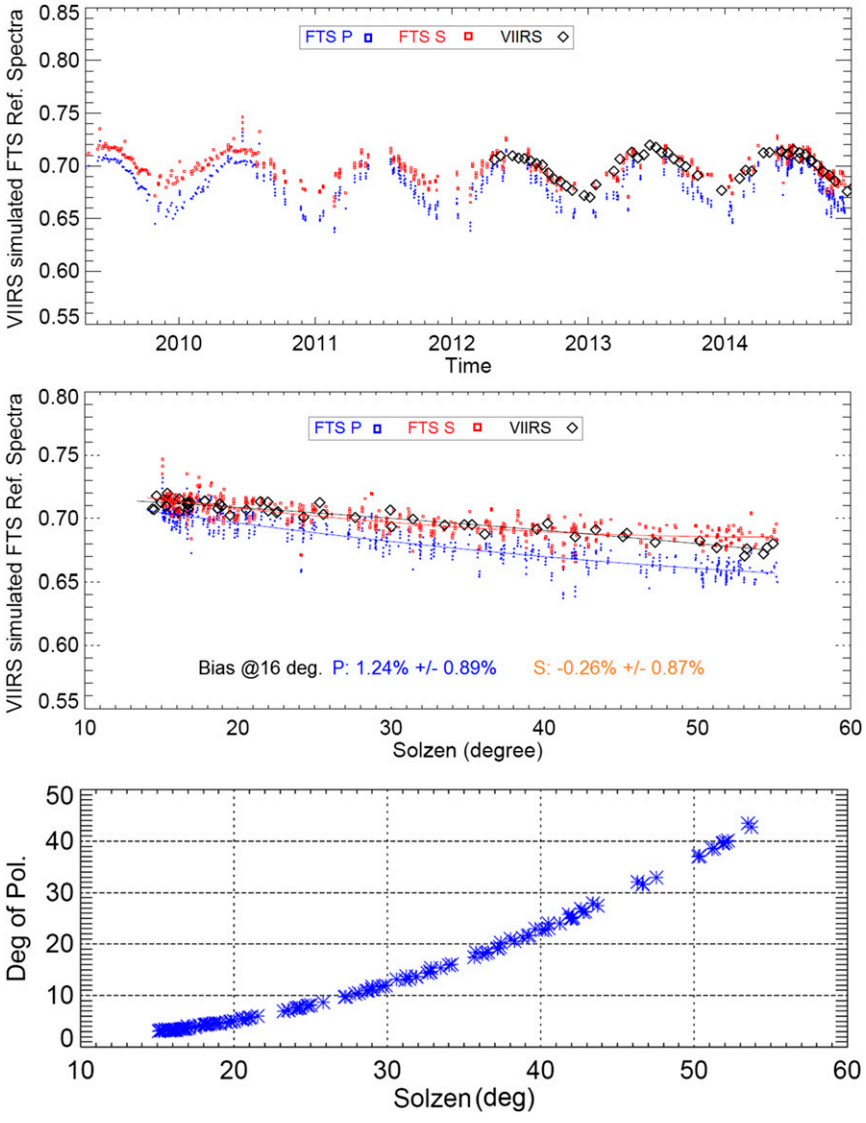

FIG. 4. (a) VIIRS and FTS TOA reflectance time series. (b) Reflectance vs solar zenith angles. (c) DOP with the changing solar zenith angle.

are not limited to a single location and thus the observations do not exactly collocate with each other. The radiometric stability is computed using linear fit. The maximum change during the period of analysis is on the order of 0.7% ± 0.9% for both *P* and *S* polarized measurements. This suggests that the instrument relative degradation is rigorously characterized and that the correction model suggested by Kuze et al. (2014) works well, making the TANSO-FTS reflectance trend very stable.

Figure 4b shows that the bias between VIIRS and TANSO-FTS varies with changing solar zenith angle. This is because, at nadir, the BRDF is strongly dominated by annual variation in the solar zenith angle. When compared to the TANSO-FTS *S* polarization, VIIRS agrees very well to within 0.3%. A larger radiometric inconsistency exists between VIIRS and *P* polarized measurements, ranging from about 1.2% at 16° solar zenith angle to nearly 3% at 55° solar zenith angle. The larger difference between *P* and *S* exists as at higher solar zenith angles mainly due to the polarization in the BRDF. A one-sigma uncertainty in bias is nearly 1% for both *P* and *S* polarization. When two instruments use different solar models to derive reflectance, it can produce a systematic bias of up to 3%. The reflectance derivation for TANSO-FTS was done using a Kuruczbased solar model; however, the VIIRS calibration is reflectance based and the TOA reflectance product is not impacted by the solar model. Because of the impact

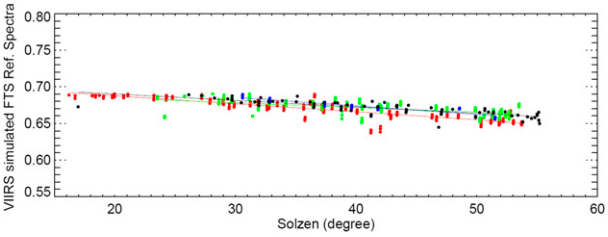

FIG. 5. Bias trends estimated at different locations observed by FTS (near the Libya-4 region). The observations are grouped into four locations indicated by four colors.

of the solar model, which was applied to convert TANSO-FTS radiance to reflectance, it is always possible to observe some level of inconsistency in the reflectance trends between VIIRS and TANSO-FTS.

The polarization is at maximum when the relative angle from the ROI to the sensor and the ROI to the sun is closer to 90°. In this study all the observations used in the analysis are collected at nadir for both VIIRS and TANSO-FTS. Thus, the viewing angle is nearly zero. However, the solar zenith over the calibration site varies from nearly 15° to 55° annually. This is one of the main reasons why the VIIRS and TANSO-FTS comparison was performed at the smallest solar zenith angles, where the impact due to polarization is almost negligible. The authors have performed the 6S radiative transfer simulation over desert sand to measure the polarization by varying the senor and the solar geometry with exactly the same values that were measured during the *GOSAT* overpass through the site. For solar zenith angles less than 20°, it was observed that the degree of polarization (DOP) of the incoming light varies from nearly 3% to 5%, which indicates that the uncertainty in intercomparison due to the polarization characteristics of the surface and atmosphere is almost negligible. Thus, the relative accuracy of VIIRS and TANSO-FTS was computed at the smallest solar zenith angle, so that there is no noticeable impact due to the polarization. Figure 4c shows the change in DOP of the incoming reflected radiance from the target with the variation in solar zenith angle. The authors agree that the impact gets larger at higher solar zenith angles due to the larger impact from polarization in the BRDF. This could be one of the reasons why the instruments suggest a larger bias at higher solar angles. In addition, Fig. 5 also indicates that a nearly 1% bias exists between the ROIs used for TANSO-FTS observations to construct the temporal reflectance series. This further adds the uncertainty in the intercomparison between the instruments. Hence, the VIIRS and TANSO-FTS comparison is performed when the uncertainties due to atmospheric BRDF, polarization, and registration errors are lowest.

The TANSO-FTS reflectance time series over desert was generated using the measurements collected from different locations. These can be grouped into four locations near the Libya-4 site. To further quantify the bias, the TANSO-FTS data collected from four locations are plotted and their differences are analyzed. Figure 5 shows that a small bias in TANSO-FTS time series exists due to a variation in the location used in the study. The trends suggest that the uncertainty in bias between VIIRS and TANSO-FTS due to TANSO-FTS target location differences is less than 1%.

It is possible to quantify the bias between VIIRS and TANSO-FTS in absolute scale traceable to *Aqua* MODIS. This can be done under the assumption that MODIS (1628–1652 μm) is correct in absolute scale. Figure 6 shows VIIRS and MODIS reflectance time series over Libya-4. The impact on bias due to spectral differences is quantified using *Earth Observing-1* (*EO-1*) Hyperion. After accounting for the spectral differences between the matching bands, VIIRS bias relative to MODIS is estimated to be 3% ± 0.7%. This indicates that the VIIRS calibration is overestimated in absolute scale by nearly 3%. Since VIIRS and TANSO-FTS agree well for *S* polarized light, it is possible that the TANSO-FTS calibration is overestimated as well. However, it is to be noted that several MODIS detectors for this band are inoperable throughout the mission. Some of the detectors are filled with interpolated values from adjacent detectors. In addition, there is uncertainty added from Hyperion-based estimation of the spectral bias in the VIIRS and MODIS comparison. The current retrieval accuracy of TANSO-FTS is 0.5%. The calibration uncertainty of the TANSO-FTS SWIR band is 7% using vicarious calibration (Kuze

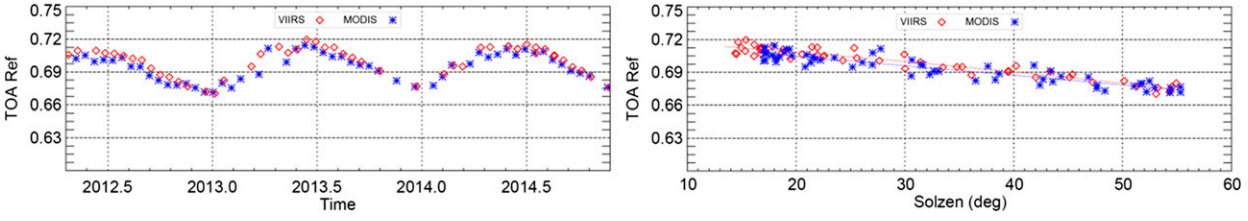

FIG. 6. Comparison of VIIRS- (1.58–1.64 μm) and MODIS- (1.628–1.652 μm) measured reflectance at the Libya-4 desert site.

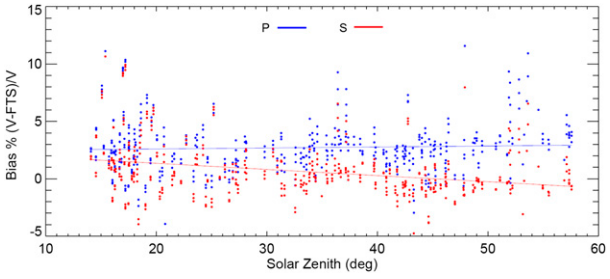

FIG. 7. FTS bias estimated using SNO-x-based intercomparison.

et al. 2014). Given the calibration uncertainty of the TANSO-FTS and VIIRS matching bands and the bias relative to each other, we cannot obtain better calibration accuracy of TANSO-FTS with VIIRS. However, the intercomparison of TANSO-FTS with VIIRS helps to independently check the long-term radiometric stability and accuracy. This independent check can provide very useful feedback to understand and confirm how well the instruments are performing over time.

b. *Extended SNO-based intercomparison over North African Desert*

Figure 7 suggests that bias for *P* polarization measurements is larger than that of *S* polarization. For each SNO event, many bias values are computed, one for each valid ROI. Bias is more scattered even for one SNO event, mainly because 1) bias is plotted for sensor zenith angles up to ±30°; 2) for each SNO event, there exists a large number of ROIs that can have slightly different spectral characteristics and atmospheric variability over which the bias is computed; 3) cloud contamination for both VIIRS and TANSO-FTS is tested using the VIIRS; 4) collocation error; 5) each bias point in the plot is estimated at different locationin the desert; and 6) the time difference of the observations, which causes the movement of clouds and possible cloud contamination in TANSO-FTS data.

The bias values observed using the extended SNO-based comparison agrees well within 1% of the bias estimated over the Libya-4 desert site, however with larger uncertainty. The uncertainty is a bias calculated as a one-sigma residual standard deviation (2.21% for *P* and 2.22% for *S* polarized light). The bias trend estimated between VIIRS and *P* polarized light has no significant slope, suggesting a mean bias of 2.7%. However, the *S* polarized light suggests a linear trend in bias ranging from nearly 1.6% to −0.7% for solar zenith angles ranging from 14° to 58°.

4. Conclusions

Comparison of *Suomi-NPP* VIIRS and *GOSAT* TANSO-FTS has been performed to evaluate the on-orbit radiometric consistency. The intersensor radiometric comparison was performed basically using two techniques, one by generating the TOA reflectance time series of both instruments near the Libya-4 desert site and comparing the reflectance trends, and the second by using the extended SNO technique over North African deserts. Intercomparison over the Libya-4 desert site suggests that VIIRS agrees with the *S* polarized measurement of TANSO-FTS very well to within 0.3%. However, the *P* polarized light indicates a larger bias ranging from 1.5% to 3% for the varying solar zenith angle with an uncertainty in bias within 1%. The discrepancy in the *P* and *S* polarized measurements needs further investigation. The extended SNO-based intercomparison over the North African desert indicates a large scatter in bias trends, increasing the uncertainty in bias to more than 2%. The biases estimated using the two techniques agree with each other to within 1%. The potential of *Aqua* MODIS as a reference standard to tie up the bias in absolute scale—that is, to a common traceable source—was also analyzed. However, MODIS has some inoperable detectors in this band. This needs more investigation in the future. The study motivates eventually helping establish a common radiometric scale between *GOSAT* TANSO-FTS and VIIRS for the 1.6-μm CO_2 band.

Acknowledgments. This work is funded by the JPSS program office under the NOAA Award NA14OAR4320125. We thank the anonymous reviewers for their constructive comments and suggestions. The manuscript contents are solely the opinion of the authors and do not constitute a statement of policy, decision, or position on behalf of NOAA or the U.S. government.

REFERENCES

Cao, C., M. Weinreb, and H. Xu, 2004: Predicting simultaneous nadir overpasses among polar-orbiting meteorological satellites for the intersatellite calibration of radiometers. *J. Atmos. Oceanic Technol.*, **21**, 537–542, doi:10.1175/1520-0426(2004)021<0537:PSNOAP>2.0.CO;2.

——, F. Deluccia, X. Xiong, R. Wolfe, and F. Weng, 2013a: Early on-orbit performance of the Visible Infrared Imaging Radiometer Suite onboard the Suomi National Polar-Orbiting Partnership (S-NPP) satellite. *IEEE Trans. Geosci. Remote Sens.*, **52**, 1142–1156, doi:10.1109/TGRS.2013.2247768.

——, J. Xiong, S. Blonski, Q. Liu, S. Uprety, X. Shao, Y. Bai, and F. Weng, 2013b: Suomi NPP VIIRS sensor data record verification, validation, and long-term performance monitoring. *J. Geophys. Res. Atmos.*, **118**, 11 664–11 678, doi:10.1002/2013JD020418.

CEOS, 2014: CEOS strategy for carbon observations from space. CEOS Carbon Task Force, JAXA and I&A Corporation, 202 pp.

Chander, G., X. Xiong, J. Choi, and A. Angal, 2010: Monitoring on-orbit calibration stability of the Terra MODIS and Landsat 7

ETM+ sensors using pseudo-invariant test sites. *Remote Sens. Environ.*, **114**, 925–939, doi:10.1016/j.rse.2009.12.003.

Helder, D. L., B. Basnet, and D. L. Morstad, 2010: Optimized identification of worldwide radiometric pseudo-invariant calibration sites. *Can. J. Remote Sens.*, **36**, 527–539, doi:10.5589/m10-085.

——, K. J. Thome, N. Mishra, G. Chander, X. Xiong, A. Angal, and T. Choi, 2013: Absolute radiometric calibration of Landsat using a pseudo invariant calibration site. *IEEE Trans. Geosci. Remote Sens.*, **51**, 1360–1369, doi:10.1109/TGRS.2013.2243738.

JAXA, 2009: GOSAT level 1 product format description document. NEB-080031, 77 pp.

Kieffer, H. H., D. A. Cook, E. M. Eliason, and P. T. Eliason, 1985: Intraband radiometric performance of the Landsat Thematic Mappers. *Photogramm. Eng. Remote Sens.*, **51**, 1331–1350.

Kina, T., K. Shiomi, S. Kawakami, Y. Mitomi, M. Yoshida, R. Higuchi, N. Sekio, and F. Kataoka, 2010: Results of calibration for GOSAT TANSO. *International Archives of the Photogrammetry, Remote Sensing and Spatial Information Sciences*, K. Kajiwara et al., Eds., Volume XXXVIII, Part 8, ISPRS, 91–93.

Kuze, A., H. Suto, M. Nakajima, and T. Hamazaki, 2009a: Thermal and near infrared sensor for carbon observation Fourier-transform spectrometer on the Greenhouse Gases Observing Satellite for greenhouse gases monitoring. *Appl. Opt.*, **48**, 6716–6733, doi:10.1364/AO.48.006716.

——, ——, K. Shiomi, M. Nakajima, and T. Hamazaki, 2009b: On-orbit performance and level 1 data processing of TANSO-FTS and CAI on GOSAT. *Sensors, Systems, and Next-Generation Satellites XIII*, R. Meynart, S. P. Neeck, and H. Shimoda, Eds., International Society for Optical Engineering (SPIE Proceedings, Vol. 7474), 74740I, doi:10.1117/12.830152.

——, and Coauthors, 2012: Level 1 algorithms for TANSO on GOSAT: Processing and on-orbit calibrations. *Atmos. Meas. Tech.*, **5**, 2447–2467, doi:10.5194/amt-5-2447-2012.

——, and Coauthors, 2014: Long-term vicarious calibration of GOSAT short-wave sensors: Techniques for error reduction and new estimates of radiometric degradation factors. *IEEE Trans. Geosci. Remote Sens.*, **52**, 3991–4004, doi:10.1109/TGRS.2013.2278696.

——, and Coauthors, 2016: Update on GOSAT TANSO-FTS performance, operations, and data products after more than 6 years in space. *Atmos. Meas. Tech.*, **9**, 2445–2461, doi:10.5194/amt-9-2445-2016.

Markham, B. L., and D. L. Helder, 2012: Forty-year calibrated record of earth-reflected radiance from Landsat: A review. *Remote Sens. Environ.*, **122**, 30–40, doi:10.1016/j.rse.2011.06.026.

Metzler, M. D., and W. A. Malila, 1985: Characterization and comparison of Landsat-4 and Landsat-5 Thematic Mapper data. *Photogramm. Eng. Remote Sensing*, **51**, 1315–1331.

Moreau, L., J. Veilleux, and H. Suto, 2014: The GOSAT/TANSO interferometer after five years on orbit. *Infrared Remote Sensing and Instrumentation XXII*, M. Strojnik Scholl and G. Páez, Eds., International Society for Optical Engineering (SPIE Proceedings, Vol. 9219), 921902, doi:10.1117/12.2067791.

Shiomi, K., S. Kawakami, T. Kina, M. Yoshida, N. Sekio, Y. Mitomi, and F. Kataoka, 2007: GOSAT calibration plan. *Proc. ENVISAT Symp. 2007*, Montreux, Switzerland, European Space Agency, ESA SP-696, 23–27. [Available online at https://earth.esa.int/envisatsymposium/proceedings/posters/3P5/462261sh.pdf.]

Slocum, G., 1955: Has the amount of carbon dioxide in the atmosphere changed significantly since the beginning of the twentieth century? *Mon. Wea. Rev.*, **83**, 225–231, doi:10.1175/1520-0493(1955)083<0225:HTAOCD>2.0.CO;2.

Teillet, P., J. Barsi, G. Chander, and K. Thome, 2007: Prime candidate Earth targets for the post-launch radiometric calibration of space-based optical imaging instruments. *Earth Observing Systems XII*, J. J. Butler and J. Xiong, Eds., International Society for Optical Engineering (SPIE Proceedings, Vol. 6677), 66770S, doi:10.1117/12.733156.

Uprety, S., C. Cao, X. Xiong, S. Blonski, A. Wu, and X. Shao, 2013: Radiometric intercomparison between *Suomi-NPP* VIIRS and *Aqua* MODIS reflective solar bands using simultaneous nadir overpass in the low latitudes. *J. Atmos. Oceanic Technol.*, **30**, 2720–2736, doi:10.1175/JTECH-D-13-00071.1.

Yoshida, Y., Y. Ota, N. Eguchi, N. Kikuchi, K. Nobuta, H. Tran, I. Morino, and T. Yokota, 2011: Retrieval algorithm for CO_2 and CH_4 column abundances from short-wavelength infrared spectral observations by the Greenhouse gases observing satellite. *Atmos. Meas. Tech.*, **4**, 717–734, doi:10.5194/amt-4-717-2011.

——, N. Kikuchi, and T. Yokota, 2012: On-orbit radiometric calibration of SWIR bands of TANSO-FTS onboard GOSAT. *Atmos. Meas. Tech.*, **5**, 2515–2523, doi:10.5194/amt-5-2515-2012.